MEASUREMENT OF INTERSTAGE FLUID-ANNULUS DYNAMICAL PROPERTIES

M. L. Adams
University of Akron
Akron, Ohio 44325

E. Makay
Energy Research & Consultants Corporation
Morrisville, Pennsylvania 19067

I. A. Diaz-Tous
EPRI
Palo Alto, California 94303

ABSTRACT

The work described in this paper is part of an Electric Power Research Institute sponsored effort to improve rotor vibrational performance on power plant feed water pumps. A major objective of this effort is to reduce vibration levels by devising inter-stage sealing configurations with optimized damping capacity, realizing that the typical multi-stage centrifugal pump has several more inter-stage fluid annuli than it has journal bearings. Also, the fluid annuli are distributed between the journal bearings where vibration levels are highest and can therefore be "exercised" more as dampers than can the bearings. Described in this paper is a test apparatus which has been built to experimentally determine fluid-annulus dynamical coefficients for various configurations of inter-stage sealing geometry.

INTRODUCTION

As originally cited in an Electric Power Research Institute survey on feedwater pump outages, Reference (1), excessive vibration is responsible for many power plant forced outages. The major cause of this excessive vibration is now widely recognized as the fluid dynamical forces generated within high-head centrifugal pump flow passages. These dynamical forces are a natural by-product of the high rate of energy transfer to the fluid within a relatively small space and the fact that this transfer of energy cannot, of course, take place at 100 percent efficiency. The farther away from the best efficiency flow a feed pump is operated, the stronger these dynamical forces become, particularly under the low-flow conditions required at part-load operation. Hydraulic excitation forces will remain an inherent feature of feed pumps. Further research on pump hydraulics may possibly reduce their intensity, but their elimination as an important practical consideration would appear to be unlikely. The most promising approach is to optimize system damping, the classical approach when the dynamical forces are not adequately controllable.

One of the approaches presently being pursued is to devise high-damping inter-stage fluid-annulus configurations, Reference (2). The typical multi-stage centrifugal pump has several more inter-stage fluid annuli than it has journal bearings (see Figure 1). Also, the fluid annuli are distributed between the journal bearings where vibration levels are highest and can therefore be exercised more as dampers than can the bearings.

As shown in Reference (3), wear-ring geometry is already known to be a potentially major influence on critical speeds. Currently used geometries are shown in Figure 2, with some type of serrations often preferred to accommodate rubs. However, some pump manufacturers have employed smooth or shallow groove geometries to utilize the resulting radial stiffening effect which can raise the first critical speed considerably above the operating speed. However, as also shown in Reference (3) (see Figure 3), this stiffening effect (called "Lomakin" effect) deteriorates with wear, which can cause high vibration levels after several hours of normal operation. In spite of the attention this potential stiffening effect has received, practically no attention has been given to the potential damping capacity of interstage fluid annuli. Raising or lowering critical speeds can not circumvent the undesireable effects of large hydraulic excitation forces but properly adjusted damping can.

ROTOR VIBRATION DAMPING EVALUATION

A linearized vibration mathematical model is generally the appropriate starting point to study and understand rotor vibration characteristics. In the presence of vibration, an interactive dynamic radial force occurs where there is a close running clearance filled with a liquid or gas (e.g., journal bearings, seals, wear-ring clearances). Such interactive forces are commonly characterized in a linear model as shown in the following matrix equation.

$$\begin{Bmatrix} f_x \\ f_y \end{Bmatrix} = - \begin{bmatrix} D_{xx} & D_{xy} \\ D_{yx} & D_{yy} \end{bmatrix} \begin{Bmatrix} \ddot{x} \\ \ddot{y} \end{Bmatrix} - \begin{bmatrix} B_{xx} & B_{xy} \\ B_{yx} & B_{yy} \end{bmatrix} \begin{Bmatrix} \dot{x} \\ \dot{y} \end{Bmatrix} - \begin{bmatrix} K_{xx} & K_{xy} \\ K_{yx} & K_{yy} \end{bmatrix} \begin{Bmatrix} x \\ y \end{Bmatrix} \tag{1}$$

Here, [K], [B] and [D] are the stiffness, damping and virtual mass matrices, respectively, of the entrapped fluid within the close-running radial clearance. (x,y) is the instantaneous rotor-to-stator radial displacement vector with respect to static equilibrium and (f_x, f_y) the instantaneous radial dynamic force vector. Presently, there is little reliable information on the dynamic matrix coefficients for feed pump fluid annuli.

To evaluate and compare damping capacity of various fluid-annulus geometries, it is a considerable simplification if harmonic motions are used. First of all, this provides a convenient way to absorb the [D] matrix into the [K] matrix as commonly done.

$$[\bar{K}] = [K] - \Omega^2[D] \tag{2}$$

Here, Ω is the frequency of the orbital vibration (see Figure 4). As described in Reference (4), the [B] and [K] matrices are non-symmetric for journal bearings and other fluid annuli contained within a rotating and non-rotating boundary. To separate out conservative and non-conservative (damping) effects, the [B] and [K] matrices are decomposed into symmetric and skew-symmetric parts.

$$[B_{ij}^s] = \frac{1}{2} [B_{ij} + B_{ji}] , \text{ symmetric (positive damping)}$$

$$[B_{ij}^{ss}] = \frac{1}{2} [B_{ij} - B_{ji}] , \text{ skew-symmetric (contributes no damping)}$$

$$[K_{ij}^{S}] = \frac{1}{2}[K_{ij} + K_{ji}] \text{ , symmetric (contributes no damping)}$$

$$[K_{ij}^{SS}] = \frac{1}{2}[K_{ij} - K_{ji}] \text{ , skew-symmetric (negative damping)} \tag{3}$$

The instantaneous non-conservative interactive force vector on the rotor can therefore be expressed as follows.

$$\{P\} = -[B^{S}]\{\dot{X}\} - [K^{SS}]\{X\} \tag{4}$$

The net energy imparted to the rotor (at a fluid annulus) per cycle of orbital motion can therefore be expressed by evaluating the integral of the non-conservative force vector, $\{P\}$, with the differential radial displacement over one period of harmonic motion, expressed as follows.

$$E_{cyc} = \oint \{P\} \cdot \{dX\}$$
$$= -\pi \left[\Omega(B_{xx}^{S}X^{2} + B_{yy}^{S}Y^{2}) - 2K_{xy}^{SS} \sin(\theta_{x} - \theta_{y})\right] \tag{5}$$

Here, x and y are the principal coordinates of $[B^{S}]$, and X and Y the corresponding single-peak amplitudes, and (θ_{x}, θ_{y}) the respective phase angles.

For any co-rotational orbit $\sin(\theta_{x} - \theta_{y}) > 0$. Furthermore, if as with journal bearings, B_{xx}^{S}, B_{yy}^{S} and K_{xy}^{SS} are all positive, one sees the presence of both positive and negative damping effects on forward whirls. It is clear from equation (5) why rotor-bearing instability always occurs as a co-rotational or forward whirling vibration.

A compact way to evaluate the net damping capacity of a fluid annulus (or journal bearing) is to determine E_{cyc} as a function of vibration-to-speed frequency ratio. For example, trends of journal bearing damping (E_{cyc}) are shown in Figure 5, which is an alternate way of explaining why rotor-bearing instability occurs when the lowest rotor-bearing resonance frequency is below the zero-damping cross-over frequency ratio. A similar approach for evaluating net damping capacity of interstage fluid annuli could be employed if the dynamic coefficients were known. Also, predictive analyses of feed pump vibration in general would be considerably advanced with reliable dynamic coefficients. A test rig has been designed and built to experimentally determine the [D], [B] and [K] matrix coefficients under operating conditions in feed water pumps.

TEST RIG AND GOVERNING EQUATIONS

Under Electric Power Research Institute sponsorship, a test rig has been designed and built to experimentally determine the dynamic coefficients of currently used and newly devised inter-stage fluid-annulus configurations. Testing is currently in progress and the results will be published when the work is completed.

A conceptual sketch of the test rig is shown in Figure 6, and a detail layout of the actual rig is shown in Figure 7. The concept employed in the design of this rig follows directly from the governing equations which relate the interactive

dynamic force components and the components of relative radial harmonic motion. As developed in Appendix A of this paper, twelve independent equations are needed which relate the force and motion parameters to the twelve dynamic coefficients. These equations are summarized below for the harmonic circular orbit, which is the vibration mode built into the test rig eccentric-spindles design.

$$(F_x \cos \theta_x)/R = - K_{xx} - \Omega_j B_{xx} + \Omega_j^2 D_{xx} - \Omega_j B_{xy}$$

$$(F_x \sin \theta_x)/R = - \Omega_j B_{xx} + K_{xy} - \Omega_j^2 D_{xy}$$

$$(F_y \cos \theta_y)/R = - K_{yx} + \Omega_j^2 D_{yx} - B_{yy}\Omega_j$$

$$(F_y \sin \theta_y)/R = - \Omega_j B_{yx} - K_{yy} - \Omega_j^2 D_{yy}$$

$$(6)$$

where, $j = 1,2,3$

The controlled parameters are X and Y, the single-peak vibration amplitudes and their respective phase angles ϕ_x and ϕ_y. The measured parameters are F_x and F_y, the single-peak dynamic force amplitudes and their respective phase angles, θ_x and θ_y. As implied by equations (6), test data is needed at three different vibration frequencies for a given operating condition. That is, one needs twelve independent equations to solve for twelve unknowns. This necessitates independent control over rotational speed and vibration orbit frequency.

There are basically two experimental approaches one could take: (i) impose dynamical forces and measure displacements, or (ii) impose dynamical displacements and measure the forces. With currently available measurement techniques, the second approach is potentially more accurate, and has been used in our design. The test rig is configured around a double-spool spindle, with the inner spindle having an adjustable run-out or eccentricity with the outer spindle (Figures 6 and 7). Rotation of the outer shaft therefore causes the rotational centerline of the inside shaft to experience a circular orbit with a precession frequency of the outside shaft's rotational speed. The rotational speed of the inside shaft is the test rotational speed. Independent control over vibration frequency and test speed is therefore accomplished. The same approach is now being used (see Reference (5)) to experimentally determine the linearized spring and damping coefficients for low specific speed centrifugal pump stages. As the shaft-to-shaft eccentricity is adjusted, it can be measured with extreme accuracy using an LVDT or even a precision dial indicator while slowly rotating the outer shaft by hand.

The test ring is rigidly supported in the radial plane by four piezoelectric load cells (see Figures 6 and 7), two in each of the x and y mutually perpendicular directions which allow variation of orbit-center eccentricity. The necessary advantage of piezoelectric load cells is that they are extremely stiff and therefore keep test ring vibration amplitudes negligible and therefore unnecessary to measure. Strain gauge load cells would not be a feasible option here because they require displacement to sense load.

The test ring is contained within a pressurized chamber. The test ring divides the chamber into high and low pressure compartments. The difference in pressure between these two compartments is controlled to the desired test pressure drop

across the fluid annulus, with a maximum axial pressure drop of 500 psi through the test annulus. The test ring is supported axially on fluid film hydrostatic thrust faces which introduce no extraneous radial loads. The test ring is attached to the four load cells by four leaf springs which are soft in the circumferential direction but stiff in the radial and axial direction. This type of construction allows the fluid reaction torque on the test ring to be equilibrated by the test ring support, without introducing extraneous radial forces on the test ring. The closure head of the pressurized chamber is easily removed as is the test ring and test journal. This provides for quick interchange of the various fluid annulus configurations to be tested and modified.

It is essential that the radial run-out of the test journals which results from inner shaft rotation be as close to zero as is possible to manufacture. This was accomplished in the final machining operation on the test journals by grinding them while they were rotated (inner shaft rotated, outer shaft fixed) in the final assembled double-shaft spindle.

For any given annulus configuration (i.e., diameter, axial width, clearance and surface geometry) the basic operating parameters are rotational speed, water temperature, static eccentricity and axial pressure drop across the test annulus. The effects of each of these parameters will be determined by varying them through ranges encountered in actual feed pump applications.

CONCLUSIONS

The importance of inter-stage fluid annuli to rotor dynamical performance of high-head feed water pumps warrants developmental efforts by the pump manufacturers in this area. The test rig described in this paper has recently come on-line and is just beginning to provide reliable data on inter-stage fluid-annulus dynamic coefficients. Currently used configurations as well as newly devised high-damping configurations are being tested. By the end of this year, we anticipate the completion of the testing that is presently planned. We expect to be able to recommend inter-stage clearance geometries which will provide considerable additional rotor vibrational damping capacity for feed water pump and other multi-stage centrifugal pump applications.

REFERENCES

1. Makay, E. and Szamody, O., "Survey of Feed Pump Outages", EPRI Publication FP-754, April 1978.

2. Adams, M. L. and Makay, E., "Development of Advanced Rotor-Bearing Systems for Feed Water Pumps, Phase 2", EPRI Publication CS-2027, September 1981.

3. Makay, E., "How Close Are Your Feed Pumps to Instability - Caused Disaster?", Power, McGraw-Hill, December 1980.

4. Adams, M. L. and Padovan, J., "Insights into Linearized Rotor Dynamics", Journal of Sound and Vibration, Vol. 76(1), May 1981.

5. Brennen, C. E., Acosta, A. J. and Caughey, T. K., "A Test Program to Measure Fluid Mechanical Whirl-Excitation Forces in Centrifugal Pumps", Proc. Texas A & M Workshop (May 1980) on Instability Problems in High-Performance Turbomachinery, NASA Conference Publication 2133, pp 229-235.

Appendix A

GOVERNING EQUATIONS WHICH RELATE EXPERIMENTAL MEASUREMENTS
TO FLUID-ANNULUS DYNAMIC COEFFICIENTS

A.1 DEVELOPMENT OF GOVERNING FORCE DISPLACEMENT EQUATION

Postulating harmonic motion, equations for rotor system vibrations can be expressed using phasor notation as follows.

$$f_x = F_x e^{i(\Omega t + \theta_x)} \quad , \quad f_y = F_y e^{i(\Omega t + \theta_y)}$$

$$x = X e^{i(\Omega t + \theta_x)} \quad , \quad y = Y e^{i(\Omega t + \theta_y)}$$

$$\dot{x} = i\Omega x \quad , \quad \dot{y} = i\Omega y \tag{A-1}$$

$$\ddot{x} = -\Omega^2 x \quad , \quad \ddot{y} = -\Omega^2 y$$

For the general linear case, the force-motion equations are given in expanded form as follows.

$$f_x = - K_{xx}x - B_{xx}\dot{x} - D_{xx}\ddot{x} - K_{xy}y - B_{xy}\dot{y} - D_{xy}\ddot{y}$$

$$f_y = - K_{yx}x - B_{yx}\dot{x} - D_{yx}\ddot{x} - K_{yy}y - B_{yy}\dot{y} - D_{yy}\ddot{y} \tag{A-2}$$

Using harmonic motion, equations (A-1), the force-motion equations (A-2) then can be simplified as follows.

$$f_x = (- K_{xx} - i\Omega B_{xx} + \Omega^2 D_{xx})x + (- K_{xy} - i\Omega B_{xy} + \Omega^2 D_{xy})y$$

$$f_y = (- K_{yx} - i\Omega B_{yx} + \Omega^2 D_{yx})x + (- K_{yy} - i\Omega B_{yy} + \Omega^2 D_{yy})y \tag{A-3}$$

Using the phasor form, (A-1), and dividing through by $e^{-i\Omega t}$ gives the following.

$$F_x e^{i\theta_x} = (- K_{xx} - i\Omega B_{xx} + \Omega^2 D_{xx})X e^{i\phi_x} +$$

$$(- K_{xy} - i\Omega B_{xy} + \Omega^2 D_{xy})Y e^{i\phi_y}$$

$$F_y e^{i\theta_y} = (- K_{yx} - i\Omega B_{yx} + \Omega^2 D_{yx})X e^{i\phi_x} + \tag{A-4}$$

$$(- K_{yy} - i\Omega B_{yy} + \Omega^2 D_{yy})Y e^{i\phi_y}$$

Recalling from basic phasor convention, $e^{i\theta} = \cos\theta + i\sin\theta$. Therefore, equations (A-4) take the following form.

$$F_x (\cos \theta_x + i \sin \theta_x) = (- K_{xx} - i\Omega B_{xx} + \Omega^2 D_{xx})X$$

$$(\cos \phi_x + i \sin \phi_x) = (- K_{xy} - i\Omega B_{xy} + \Omega^2 D_{xy})Y$$

$$(\cos \phi_y + i \sin \phi_y)$$

$$F_y (\cos \theta_y + i \sin \theta_y) = (- K_{yx} - i\Omega B_{yx} + \Omega^2 D_{yx})X$$

$$(\cos \phi_x + i \sin \phi_x) + (- K_{yy} - i\Omega B_{yy} + \Omega^2 D_{yy})Y$$

$$(\cos \phi_y + i \sin \phi_y) \tag{A-5}$$

The two complex equations of (A-5) can be segregated by real and imaginary parts to obtain four real equations. Since there are twelve unknowns (i.e., the stiffness, damping and inertia coefficients), experimentally measured inputs to these equations must be obtained at three different vibration frequencies (i.e., Ω_j, $j = 1,2,3$) for a given operating condition. This leads to the following general form of the governing equations.

$$F_x \cos \theta_x = [(\Omega_j^2 D_{xx} - K_{xx}) \cos \phi_x + B_{xx}\Omega_j \sin \phi_x]X$$

$$+ [(\Omega_j^2 D_{xy} - K_{xy}) \cos \phi_y + B_{xy}\Omega_j \sin \phi_y]Y$$

$$F_x \sin \theta_x = [(\Omega_j^2 D_{xx} - K_{xx}) \sin \phi_x - B_{xx}\Omega_j \cos \phi_x]X$$

$$+ [(\Omega_j^2 D_{xy} - K_{xy}) \sin \phi_y - B_{xy}\Omega_j \cos \phi_y]Y$$

$$F_y \cos \theta_y = [(\Omega_j^2 D_{yx} - K_{yx}) \cos \phi_x + B_{yx}\Omega_j \sin \phi_x]X$$

$$+ [(\Omega_j^2 D_{yy} - K_{yy}) \cos \phi_y + B_{yy}\Omega_j \sin \phi_y]Y$$

$$F_y \sin \theta_y = [(\Omega_j^2 D_{yx} - D_{yx}) \sin \phi_x - B_{yx}\Omega_j \cos \phi_x]X$$

$$+ [(\Omega_j^2 D_{yy} - K_{yy}) \sin \phi_y - B_{yy}\Omega_j \cos \phi_y)Y \tag{A-6}$$

where, $j = 1,2,3$.

As explained in the main text of this paper, the test rig has been designed to provide a controlled harmonic circular orbit of radius R. That is,

$$X = Y = R \text{ and } \phi_y = \phi_x - \frac{\pi}{2}$$

Therefore, $\cos \phi_y = \sin \phi_x$ and $\sin \phi_y = - \cos \phi_x$. Furthermore, all phase angles can be referenced to the x-component of vibration (i.e., $\phi_x \equiv 0$). Implementing all these simplifications, reduces equations (A-6) to the following.

153

$$(F_x \cos \theta_x)/R = -K_{xx} - \Omega_j B_{xx} + \Omega_j^2 D_{xx} - \Omega_j B_{xy}$$

$$(F_x \sin \theta_x)/R = -\Omega_j B_{xx} + K_{xy} - \Omega_j^2 D_{xy}$$

$$(F_y \cos \theta_y)/R = -K_{yx} + \Omega_j^2 D_{yx} - B_{yy}\Omega_j$$

$$(F_y \sin \theta_y)/R = -\Omega_j B_{yx} - K_{yy} - \Omega_j^2 D_{yy} \tag{A-7}$$

where, $j = 1,2,3$

A.2 EXPERIMENTAL ERROR CONSIDERATIONS

Equations (A-7) provide twelve equations in twelve unknowns. The orbit of vibration, R, and its frequency are controlled by the design of the test rig. The single-peak dynamic force amplitudes (F_x, F_y) and the associated dynamic force phase angles (θ_x, θ_y) are measured. The remaining twelve unknowns are the dynamic coefficients. Close examination of equations (A-7) will reveal that the first two sets of equations are coupled only to each other, while the third and fourth sets of equations are individually decoupled from the other equation sets. This is a result of the basic approach of using a controlled circular orbit vibration. An additional advantage is thereby provided since one does not have to actually solve a single system of twelve equations. Instead, solution requires individual solution of one system of six equations and two systems of three equations. This simplification tends to reduce the affinity for amplification of experimental error in the equation solution step of the overall scheme for determining the dynamic coefficients.

As fully shown, experimental data is required at three different frequencies for a specific operating condition in order to recover the twelve dynamic coefficients from the governing equations. Therefore, in theory, any three sufficiently different frequencies should yield the same dynamic coefficients for a given operating condition. The experimental setup therefore inherently provides a means for determining the overall inaccuracy of the experimentally determined coefficients. That is, one can obtain data at say ten (or more) different vibration frequencies and then determine the dynamic coefficients with the data from all unique combinations of three different frequencies out of the total of ten (or more) frequencies available. The difference in answers between the different combinations is the experimental spread or error. Experimental error will come from two basic sources: (i) measurement inaccuracies, and (ii) non-linearity in the actual force-displacement phenomenon. These two sources of error will tend to work in opposition. That is, measurement inaccuracies can be minimized by using "larger" vibration amplitudes, thus making the measured response forces larger and therefore easier to measure accurately. However, the larger the vibration amplitude, the more significant becomes the non-linearities, which are neglected in the governing equations. Therefore, for each operating condition there will be an optimum orbital vibration radius which minimizes the experimental error, being large enough to obtain good measurements, but not too large to produce significant non-linearities. The test rig spindle is designed to that the orbital vibration radius can be varied, specifically so that error can be minimized.
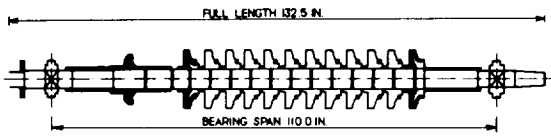
Figure 1. - Twelve-stage boiler feed pump rotor; cane run no. 6 station, Louisville gas and electric.
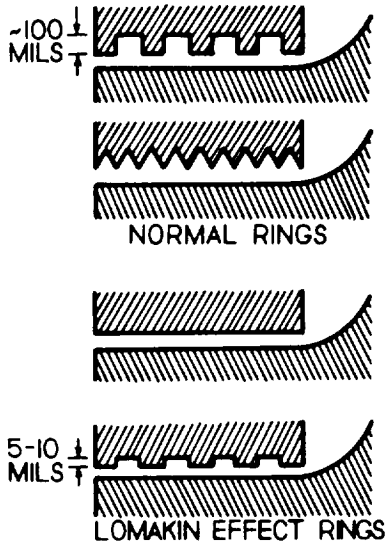

Figure 2. - Currently used feed pump wear ring geometries, reference (3).
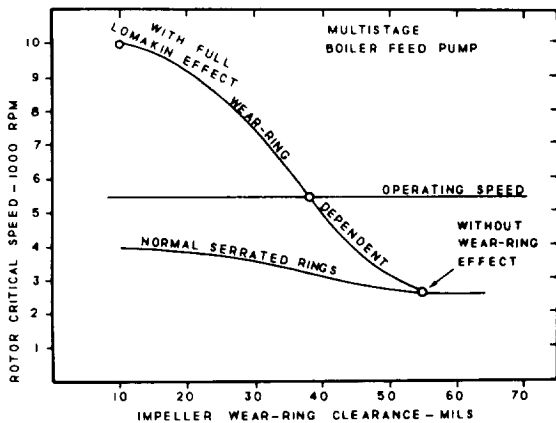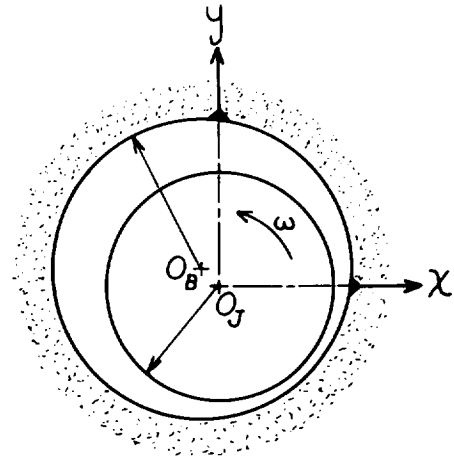

Figure 3. - Lomakin effect on first critical speed of a typical feed water pump, reference (3).

Figure 4. - Single-frequency harmonic orbital vibration of rotor with respect to stator.
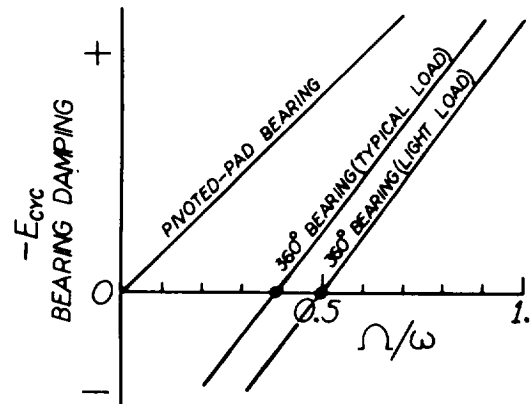
Figure 5. - Trends of journal bearing net damping per cycle of harmonic motion. Ω/ω is vibration frequency-to-speed ratio.

155
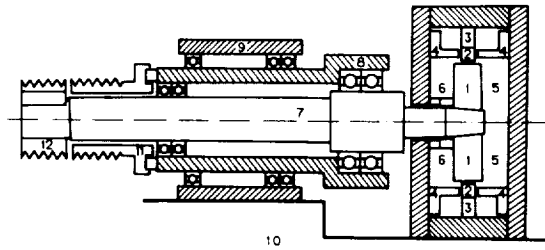
Legend:

1 - Test rotating element
2 - Test annulus ring
3 - Piezoelectric load cell
4 - Hydrostatic axial ring support
5 - High-pressure compartment
6 - Low-pressure compartment

7 - Inner spindle rotor
8 - Outer spindle rotor
9 - Spindle housing
10 - Support base
11 - V-belt pulley
12 - V-belt pulley

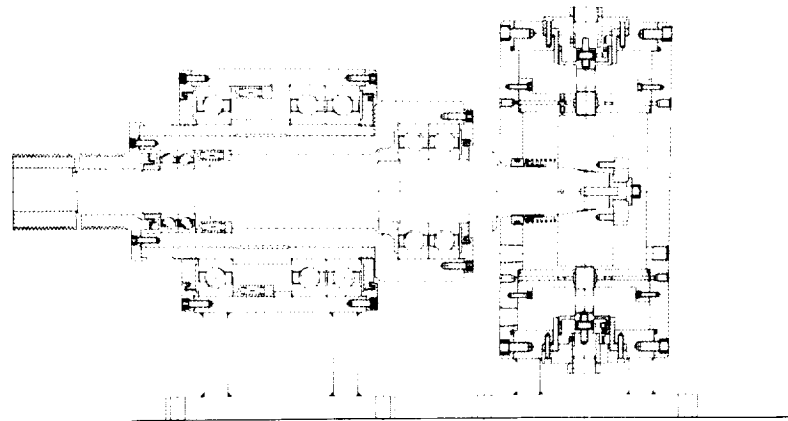Figure 6. - Conceptual sketch of double-spool spindle fluid-annulus test rig.

Figure 7. - Detail layout of double-spool spindle fluid-annulus test rig.

156